Optimal population transfer using adiabatic rapid passage in the presence of drive-induced dissipation

Nilanjana Chanda [1,*] Pratik Patnaik [2,†] and Rangeet Bhattacharyya [1,‡]

[1]*Department of Physical Sciences, Indian Institute of Science Education and Research Kolkata, Mohanpur 741246, West Bengal, India*

[2]*Colorado School of Mines, 1500 Illinois St, Golden, Colorado 80401, USA*

(Received 24 January 2023; accepted 12 June 2023; published 23 June 2023)

Adiabatic rapid passage (ARP) is extensively used to achieve efficient transfer or inversion of populations in quantum systems. Landau and Zener accurately estimated the transfer probability of ARP for a closed system and showed that this probability improved with higher drive amplitude. Recently, we found that, in open quantum systems, applying a strong drive can give rise to significant drive-induced dissipation (DID). Here, we investigate the effect of DID on the performance of ARP that is implemented using a linearly chirped pulse on a two-level system. From the Landau-Zener formula, the population transfer was known to be enhanced with increasing drive amplitude. However, here we show that, beyond a threshold value of the drive amplitude, the transfer probability is reduced because of the detrimental effect of DID. We show that the competition between the two processes results in an optimal behavior of the population transfer. We also propose a phenomenological model that helps explain such nonmonotonic behavior of the transfer. Using this model, we estimate the optimum time at which the maximum population transfer occurs. We extend the analysis for rectangular as well as Gaussian pulse profiles and conclude that a Gaussian pulse outperforms a rectangular pulse.

DOI: 10.1103/PhysRevA.107.063708

I. INTRODUCTION

Adiabatic rapid passage (ARP) is an efficient and robust method for population transfer between two levels of a quantum system. ARP commonly involves applying a chirped pulse across the resonance frequency of two specific energy levels of a quantum system. The chirped pulse, usually symmetric, covers a wide frequency range, with endpoints far away from the resonance. If the sweep is sufficiently slow to satisfy the *adiabaticity* criterion, then populations of the concerned levels undergo complete inversion with 100% efficiency. In the early 1930s, Landau provided a theoretical description of the process, which Zener perfected soon after [1–3]. Since the 1970s, it is commonly referred to as the Landau-Zener theory [4–7]. According to them, if the adiabaticity criterion is not maintained during the sweep, there is a possibility that the system could make a transition from one eigenstate to the other. This is known as the Landau-Zener (LZ) transition, which is a nonadiabatic transition. As a result, ARP and LZ transition are two complementary processes and the probability of the population transfer in ARP follows from the LZ formula, as we shall discuss in detail in the next section.

For a linearly chirped drive of constant amplitude ω_1 and frequency sweep rate R, the *adiabaticity* condition requires $R/\omega_1 \ll \omega_1$ [8]. To achieve an efficient transfer, free from the effects of the environment the process must be executed fast enough compared to the timescale of relaxation T_R of the quantum system. As such, this passage is *fast* or *rapid*. The two requirements can be combined as $\frac{1}{T_R} \ll \frac{R}{\omega_1} \ll \omega_1$. The first inequality is the requirement for *rapid*, whereas the second is the requirement for *adiabaticity*. So, it is evident that the application of a higher drive amplitude is preferable for more efficient transfer. This condition also follows from the LZ formula.

As an experimental technique, ARP has been known since its seminal use by Bloch, Hansen, and Packard to detect nuclear magnetic resonance [9]. Since then, through the works of Redfield, Abragam, Proctor, Slichter, and others, ARP emerged as a useful technique for the population inversion, adiabatic demagnetization, spin temperature studies, and others [10–15]. In recent times, ARP has been extensively used in population transfer, wavelength conversions, quantum computing, and others [16–20].

In addition to magnetic resonance, ARP has also been used in optical regimes using frequency-swept laser pulses [21–23]. Melinger *et al.* demonstrated that, when applied in the adiabatic limit, frequency-swept picosecond laser pulses could be used to achieve efficient population transfer by ARP in two-level and multilevel systems [22]. A few years later, Malinovsky *et al.* presented a general theory of ARP with intense, linearly chirped laser pulses [23]. They derived a modified LZ formula to determine the optimal conditions for efficient and robust population transfer. Maeda *et al.* reported coherent population transfer between Rydberg states of Li atoms by higher-order multiphoton ARP [24]. Instead of using a sequence of ARPs of single-photon transitions, they used ARP of a single multiphoton transition.

*nc16ip020@iiserkol.ac.in
†pratikpatnaik@mines.edu
‡rangeet@iiserkol.ac.in

 ©2023 American Physical Society

ARP has also been studied on systems where the "rapid" criterion is not completely satisfied [25–31]. In such systems, the effect of the relaxation on the transfer efficiency is not negligible. Nalbach and others investigated LZ transition in a dissipative environment [28]. They showed a nonmonotonic dependence of the transition probability on the sweep speed due to competition between relaxation and the external sweep. They explained it in terms of a simple phenomenological model. Sun *et al.* investigated finite-time LZ processes in the presence of an environment, modeled by a broadened cavity mode at zero temperature [30]. They numerically studied the survival fidelity of adiabatic states. They showed that the fidelity of the transfer exhibits a nonmonotonic dependence on the system-environment coupling strength and the sweep rate of the energy bias. Both works hint that the transfer efficiency may be optimal in the case of dissipative dynamics.

We note that a strong chirped pulse favors the ARP condition; the LZ formula of transfer also supports it. For a commonly employed linearly chirped drive of constant amplitude ω_1 and sweep rate R, both the conditions imply $\omega_1^2 \gg R$ [8]. However, we note that a strong drive gives rise to significant excitation-induced dissipation or drive-induced dissipation (DID) in open quantum systems. Although the volume of works mentioned above incorporates the dissipation due to system-environment coupling, they did not consider the drive-induced dissipation. In this work, we incorporate the DID to study the population transfer using ARP in a two-level system (TLS) coupled to its environment. To this end, we use a fluctuation-regulated quantum master equation (FRQME); a recently proposed Markovian quantum master equation that can estimate the DID [32]. We choose the parameters to mimic a nearly closed system. Thus, for our system, DID is stronger than the relaxation rate processes arising from system-environment coupling. Under this condition, we show that the population transfer has an optimal dependence on ω_1. We estimate the critical value and provide a condition for an optimal transfer using a phenomenological model. We propose that to achieve the maximum population transfer, we need to stop the drive at that very point of time when the optimal transfer is achieved. If we wait any longer, the transfer will start to decay due to the DID. The analysis is carried out for two commonly used pulse profiles, the rectangular and Gaussian, and we analyze the relative merits of their use in population transfer.

We organize the remaining part of the article in the following order. In Sec. II, we introduce our frequency sweep model to deal with the problem and describe the mathematical construction of our work. In Sec. III, we show the results. In this section, we also propose a phenomenological model to explain the optimal behavior of population transfer in the presence of DID. In Sec. IV, we discuss the implications of our work. Section V summarizes the major findings and draws final conclusions.

II. MODEL AND METHOD

As is the common practice to emulate ARP, we use a frequency sweep model. We note that Bloch and others originally proposed the feasibility of this process [9]. In the past, many used this model to study ARP. Rubbmark *et al.* used various sweep functions and checked how the energy diagram changes with each sweep [33]. Others used frequency sweep for efficient population transfer via ARP [22–24].

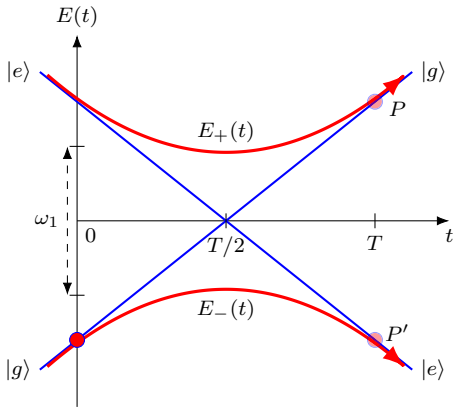

FIG. 1. The plot shows the diabats, denoted by blue straight lines and adiabats, denoted by red hyperbola. For a perfect adiabatic sweep, the system stays on the adiabat. So it can start asymptotically on a diabat $|g\rangle$ at $t = 0$ and move adiabatically along the $E_-(t)$ adiabat to reach $|e\rangle$ at $t = T$. The Landau-Zener formula gives the transition probability to move from one adiabat to another. The solid red filled circle (color online) depicts a system at state $|g\rangle$ initally. The pale red filled circles on the adiabats $E_+(t)$ and $E_-(t)$, at $t = T$ represent the final state of the system with probabilities P and P', respectively.

Before we add the dissipative effects, we describe the model and its characteristics. We consider a spin-1/2 system subjected to a linearly chirped drive swept across the resonance frequency. In the rotating frame of the drive, the Hamiltonian of the system under this process takes the form

$$H^*_{\rm tot} = -\Delta\omega(t) I_z + \omega_1 I_x, \tag{1}$$

where the frequency offset is taken as, $\Delta\omega(t) = Rt - \delta\omega$, $R = 2\delta\omega/T$ is the sweep rate with T being the duration of the sweep, $I_\alpha = \sigma_\alpha/2$, with σ_α being the Pauli matrix for α component, and ω_1 is the drive amplitude. In Eq. (1) and in the subsequent parts, the superscript "$*$" stands for representations in the rotating frame of the drive.

The eigenvalues of the above Hamiltonian are given by

$$E_\pm(t) = \pm\tfrac{1}{2}\sqrt{(Rt - \delta\omega)^2 + \omega_1^2} = \pm\tfrac{1}{2}\sqrt{\Delta\omega^2(t) + \omega_1^2}\,. \tag{2}$$

The asymptotes for the hyperbola $E_\pm(t)$ are as follows:

$$E_\pm(t) = \pm\frac{1}{2}(Rt - \delta\omega) = \pm\frac{\Delta\omega(t)}{2}. \tag{3}$$

Figure 1 shows $E_\pm(t)$ versus t plot. In this figure, we observe that the energy curves form a set of hyperbolas and the asymptotes of this hyperbola follow Eq. (3). Let us define the asymptotes $E_g = \frac{\Delta\omega(t)}{2}$ and $E_e = -\frac{\Delta\omega(t)}{2}$ as the ground state $|g\rangle$ and the excited state $|e\rangle$ energies, respectively.

Suppose the system initially lies in the ground state $|g\rangle$ and the perturbing chirped drive is turned on. From Fig. 1, we can infer the dynamics of the system. In this figure, the red curves that denote the energy eigenvalues $E_\pm(t)$ of the total Hamiltonian $H^*_{\rm tot}$ form a hyperbola and are referred to as the *adiabats*. Since the two energy curves do not cross each other,

there is always a minimum gap of ω_1 between them, it is called an *avoided crossing*. The *diabats*, i.e., the straight blue lines, are asymptotes of this hyperbola. They represent the energy eigenvalues of the unperturbed system. In the *adiabatic* limit $R \ll \omega_1^2$, the system follows the instantaneous eigenstate and stays in the same *adiabat* it started in, according to the adiabatic theorem. As a result, the system finally ends up in the other level $|e\rangle$. This demonstrates the use of ARP to transfer the population from one level to the other in a TLS. But if the sweep rate R is very high compared to ω_1, i.e., if $R \gg \omega_1^2$, then the system can make a transition from one energy eigenlevel $[E_\pm(t)]$ to the other, which is the nonadiabatic Landau-Zener transition.

In our notation, Zener's formula [1] for the probability of the LZ transition can be expressed as

$$P = \exp\left(-\frac{\pi\omega_1^2}{2R}\right). \tag{4}$$

Therefore, the probability of following the same *adiabat* would be

$$P' = 1 - P = 1 - \exp\left(-\frac{\pi\omega_1^2}{2R}\right). \tag{5}$$

In other words, P' also indicates the probability of population transfer from one level $|g\rangle$ to the other level $|e\rangle$ using ARP.

A. Fluctuation-regulated quantum master equation

In this formulation, we consider a driven quantum system connected to its environment, which is part of a larger heat bath, assumed to be in thermal equilibrium. Further, we consider that this bath experiences thermal fluctuations originating from collisional processes. We describe the system-environment pair by the following Hamiltonian:

$$\mathcal{H}(t) = \mathcal{H}_{\rm S}^{\circ} + \mathcal{H}_{\rm E}^{\circ} + \mathcal{H}_{\rm SE} + \mathcal{H}_{\rm S}(t) + \mathcal{H}_{\rm E}(t), \tag{6}$$

where $\mathcal{H}_{\rm S}^{\circ}$ is the time-independent Hamiltonian of the system, $\mathcal{H}_{\rm E}^{\circ}$ is the time-independent Hamiltonian of the environment, $\mathcal{H}_{\rm SE}$ is the coupling between the system and the environment, $\mathcal{H}_{\rm S}(t)$ represents the other system Hamiltonians including the external drive applied to the system, and $\mathcal{H}_{\rm E}(t)$ denotes the fluctuations in the environment. We model the Hamiltonian $\mathcal{H}_{\rm E}(t)$ as the stochastic fluctuations of the energy levels of $\mathcal{H}_{\rm E}^{\circ}$, and chose it to be diagonal in the eigenbasis $\{|\phi_j\rangle\}$ of $\mathcal{H}_{\rm E}^{\circ}$, as represented by $\mathcal{H}_{\rm E}(t) = \sum_j f_j(t)|\phi_j\rangle\langle\phi_j|$, where the $f_j(t)$s are modeled as Gaussian, δ-correlated stochastic variables with zero mean and standard deviation κ.

The fluctuation-regulated quantum master equation (FRQME) was introduced a few years back to incorporate the thermal fluctuations of the environment in the dynamics. Chakrabarti and others provided the complete derivation of the FRQME elsewhere [32]; as such, we provide a brief sketch of the derivation. To derive the master equation, one needs to start from the coarse-grained Liouville–von Neumann equation in the interaction representation of $(\mathcal{H}_{\rm S}^{\circ} + \mathcal{H}_{\rm E}^{\circ})$ as

$$\rho_{\rm S}(t + \Delta t) = \rho_{\rm S}(t) - i\int_t^{t+\Delta t} dt_1 \;\; {\rm Tr}_{\rm E}[H_{\rm eff}(t_1), \rho(t_1)], \tag{7}$$

where $\rho_{\rm S}$ denotes the reduced density matrix of the system, Δt is the coarse-graining interval, ${\rm Tr}_{\rm E}$ denotes the partial trace operation on the environmental degrees of freedom, $H_{\rm eff}(t) = H_{\rm S}(t) + H_{\rm SE}(t)$, and ρ is the full density matrix of the system and the environment. We note that the Hamiltonian $\mathcal{H}_{\rm E}(t)$ is absent in the commutator because of the partial trace taken over E. The density matrix inside the commutator at time t_1 can be written as, $\rho(t_1) = U(t_1, t)\rho(t)U^\dagger(t_1, t)$, where $U(t_1, t)$ denotes the propagator for the system and environment pair from time t to t_1 in the Hilbert space and is estimated as

$$U(t_1, t) \approx U_{\rm E}(t_1, t) - i\int_t^{t_1} H_{\rm eff}(t_2)U_{\rm E}(t_2)dt_2, \tag{8}$$

where $U_{\rm E}(t_1, t)$ is a finite propagator for evolution solely under fluctuations, and is given by $\mathcal{T}\exp[-i\int_t^{t_1} dt_2\, H_{\rm E}(t_2)]$, with $\mathcal{T}$ denoting the Dyson time-ordering operator. In the construction of the propagator $U(t_1, t)$, it is assumed that, $(t_1 - t) \ll \tau_s$, where τ_s denotes the timescale of the system dynamics and $\tau_s \sim {\omega_1}^{-1}, {\omega_{\rm SE}}^{-1}$, where $\omega_{\rm SE}$ is the system-environment coupling strength. As such, $U(t_1, t)$ captures a finite propagation under the environmental fluctuations and an infinitesimal propagation under the system Hamiltonian and the system-environment coupling.

Using the standard Born-Markov and time coarse-graining approximations, we would finally arrive at the following equation:

$$\begin{aligned}\frac{d}{dt}\rho_{\rm S}(t) = &-i\,{\rm Tr}_{\rm E}\big[H_{\rm eff}(t), \rho_{\rm S}(t)\otimes\rho_{\rm E}^{\rm eq}\big]^{\rm sec} \\ &- \int_0^{\infty} d\tau\; {\rm Tr}_{\rm E}\big[H_{\rm eff}(t), \big[H_{\rm eff}(t-\tau), \rho_{\rm S}(t)\otimes\rho_{\rm E}^{\rm eq}\big]\big]^{\rm sec} \\ &\times e^{-\frac{|\tau|}{\tau_c}}\end{aligned} \tag{9}$$

and we call it the fluctuation-regulated quantum master equation (FRQME) [32]. Here, the superscript "sec" denotes the secular approximation that involves ignoring the fast oscillating terms in the quantum master equation. We note that in Eq. (9), $H_{\rm eff}$ containing the drive as well as the system-environment coupling Hamiltonians, appears in both first- and second-order terms. The drive appearing in the second-order term causes dissipation in the dynamics of the system, which is known as drive-induced dissipation (DID), and has been experimentally verified [34]. Recently, we explored the effect of the DID in quantum computation [35], in quantum foundations [36], in quantum optics [37], and in quantum storage [38].

The other dissipator from the system-environment coupling term gives rise to the regular relaxation phenomenon. Both these dissipators lead to nonunitary dynamics of the system. Since we assume that ${\rm Tr}_{\rm E}\{\mathcal{H}_{\rm SE}\rho_{\rm E}^{\rm eq}\} = 0$, the system-environment coupling does not appear in the first order and the cross terms between $\mathcal{H}_{\rm S}$ and $\mathcal{H}_{\rm SE}$ also vanish.

We note that the environmental fluctuations provide an exponential regulator in the dissipator. The characteristic timescale of the decay of the autocorrelations of the fluctuations (τ_c) is assumed to be much shorter than the timescale over which the system evolves, i.e., $\tau_c \ll \tau_s$. Also, we note that FRQME is derived under another assumption of timescale separation, which is used in constructing the propagator.

Therefore, for the applicability of the FRQME, one must choose the coarse-graining interval Δt such that the following condition is satisfied: $\tau_c \ll \Delta t \ll {\omega_1}^{-1}, {\omega_{\rm SE}}^{-1}$, which can also be expressed as $\omega_1\tau_c \ll 1, \omega_{\rm SE}\tau_c \ll 1$. For the present study involving frequency sweep, we assume that the relaxation timescales are very long. Therefore, the defining criterion is as follows: $\tau_c \ll [\omega_1^2 + \Delta\omega^2(t)]^{-1/2}$.

Next, we move to the rotating frame of the drive for the sake of algebraic simplicity. In this frame, the FRQME takes the following form:

$$\frac{d\rho_{\rm s}^*}{dt} = -i\,[H_{\rm tot}^*, \rho_{\rm s}^*(t)] - \tau_c[H_{\rm s}^*(t), [H_{\rm s}^*(t), \rho_{\rm s}^*(t)]] - \mathcal{D}_{\rm SE}[\rho_{\rm s}^*(t)], \tag{10}$$

provided we assume that $H_{\rm s}(t)$ is a slowly varying function of time such that we can approximate $H_{\rm s}(t-\tau)$ by $H_{\rm s}(t)$. This assumption is commensurate with the adiabaticity condition. Here $\mathcal{D}_{\rm SE}[\rho_{\rm s}^*(t)]$ represents the dissipator arising from the corresponding double commutator term involving $H_{\rm SE}$.

Equation (10) can be expressed in the Liouville space as follows:

$$\frac{d\hat{\rho}_{\rm s}^*}{dt} = \left[-i\hat{\hat{\mathcal{L}}}^{(1)} - \hat{\hat{\mathcal{L}}}^{(2)}_{\rm drive} - \hat{\hat{\mathcal{L}}}^{(2)}_{\rm system-env.}\right]\hat{\rho}_{\rm s}^* = \hat{\hat{\Gamma}}\,\hat{\rho}_{\rm s}^*, \tag{11}$$

where $\hat{\hat{\mathcal{L}}}^{(1)}$ is the Liouville superoperator or Liouvillian for the corresponding $[H_{\rm tot}^*, \rho_{\rm s}^*(t)]$ term in the master equation. $\hat{\hat{\mathcal{L}}}^{(2)}_{\rm drive}$ and $\hat{\hat{\mathcal{L}}}^{(2)}_{\rm system-env.}$ are the second-order Liouville superoperator from the drive and system-environment coupling, respectively. The role played by $\hat{\hat{\mathcal{L}}}^{(2)}_{\rm system-env.}$ is to restore the equilibrium population and to destroy the coherences. Without assuming a specific model for $\mathcal{H}_{\rm SE}$, this process of relaxation is included in the Liouvillian through the parameters M_0, T_1, and T_2, where M_0 is the equilibrium magnetization and T_1 and T_2 denote the longitudinal and transversal relaxation times, respectively. In the absence of the drive, i.e., when $\omega_1 = 0$, $\hat{\hat{\mathcal{L}}}^{(2)}_{\rm system-env.}$ ensures that the steady-state system density matrix is given by $\begin{pmatrix} \frac{1+M_0}{2} & 0 \\ 0 & \frac{1-M_0}{2} \end{pmatrix}$.

With the explicit form of the complete superoperator, $\hat{\hat{\Gamma}}$ in Eq. (11) can be expressed as follows:

$$\frac{d}{dt}\begin{pmatrix} \rho_{\rm s,11}^* \\ \rho_{\rm s,12}^* \\ \rho_{\rm s,21}^* \\ \rho_{\rm s,22}^* \end{pmatrix} = \begin{pmatrix} -\frac{\omega_1^2\tau_c}{2} - \frac{1-M_0}{T_1} & \xi & \xi^\star & \frac{\omega_1^2\tau_c}{2} + \frac{1+M_0}{T_1} \\ \xi & -\frac{\omega_1^2\tau_c}{2} + \chi(t) - \frac{2}{T_2} & \frac{\omega_1^2\tau_c}{2} & \xi^\star \\ \xi^\star & \frac{\omega_1^2\tau_c}{2} & -\frac{\omega_1^2\tau_c}{2} - \chi(t) - \frac{2}{T_2} & \xi \\ \frac{\omega_1^2\tau_c}{2} + \frac{1-M_0}{T_1} & \xi^\star & \xi & -\frac{\omega_1^2\tau_c}{2} - \frac{1+M_0}{T_1} \end{pmatrix}\begin{pmatrix} \rho_{\rm s,11}^* \\ \rho_{\rm s,12}^* \\ \rho_{\rm s,21}^* \\ \rho_{\rm s,22}^* \end{pmatrix}. \tag{12}$$

Here, $\xi = i\omega_1/2$ and $\chi(t) = i\Delta\omega(t)$ are the first-order terms, $\omega_1^2\tau_c$ represents the second-order DID terms, and the terms involving M_0, T_1, and T_2 are the second-order relaxation terms coming from the system-environment coupling. In this work, we choose very large relaxation times (T_1 and T_2) such that $\hat{\hat{\mathcal{L}}}^{(1)}$ and $\hat{\hat{\mathcal{L}}}^{(2)}_{\rm drive}$ predominantly govern the dynamics of the system.

III. RESULTS AND ANALYSIS

We solved the FRQME (12) numerically and obtained the final system density matrix at the end of the application of the frequency sweep. We study the frequency sweep using two commonly used pulse profiles, *viz.* rectangular and Gaussian.

A. Rectangular pulse profile

First, we shall consider that the applied drive has a rectangular pulse profile with a constant amplitude ω_1. Let us consider that the system's initial state is $|g\rangle$. We take the parameter values as follows: $\delta\omega = 10\,{\rm k\,rad/s}, \omega_1 = 1\,{\rm k\,rad/s}$, $R = 0.1\,{\rm ms}^{-2}$. We remain close to the adiabatic limit as per our chosen parameter values. That means we are sweeping the drive frequency very slowly. As a result, the system stays in the same eigenstate (*adiabat*) at every instant.

In Fig. 2(a), we plot the population as a function of time. The light blue line denotes the unitary case. From the plot, we infer that the entire population is initially in the ground state. During the sweep, the ground-state population starts decreasing. On the other hand, the excited-state population grows up, and finally, at the end of the sweep the excited-state population reaches 1. This shows that we achieved a complete population transfer from the ground state to the excited state. If the adiabaticity condition were not met in choosing the parameter values, the excited-state population would be less than 1, and we could not achieve the complete transfer.

The dark blue line in Fig. 2(a) represents the population versus time plot for the DID case with $\tau_c = 10^{-2}$ ms. We observe that the population transfer is affected by DID, and the maximum transfer is reduced depending upon the values of ω_1 and τ_c chosen. The transfer profile shows a nonmonotonic behavior. At first, the excited-state population increases with time, then it reaches the maximum, and after that, its value drops with time and eventually approaches the steady-state value $\rho_{\rm s,11} = \rho_{\rm s,22} = 0.5$, as DID causes the saturation of the spin-1/2 system. It is apparent that there is a substantial loss in transfer in the asymptotic limit. We focus on achieving the optimal transfer even in the presence of the adverse effect of DID. For that, one needs to to turn off the frequency sweep (the drive) at the very moment when the maximum transfer is acquired. To predict the position of that optimal point, we propose a phenomenological model in the later part of the paper.

We can describe the dynamics using the nutating magnetization. In the rotating frame of the drive, there are effectively

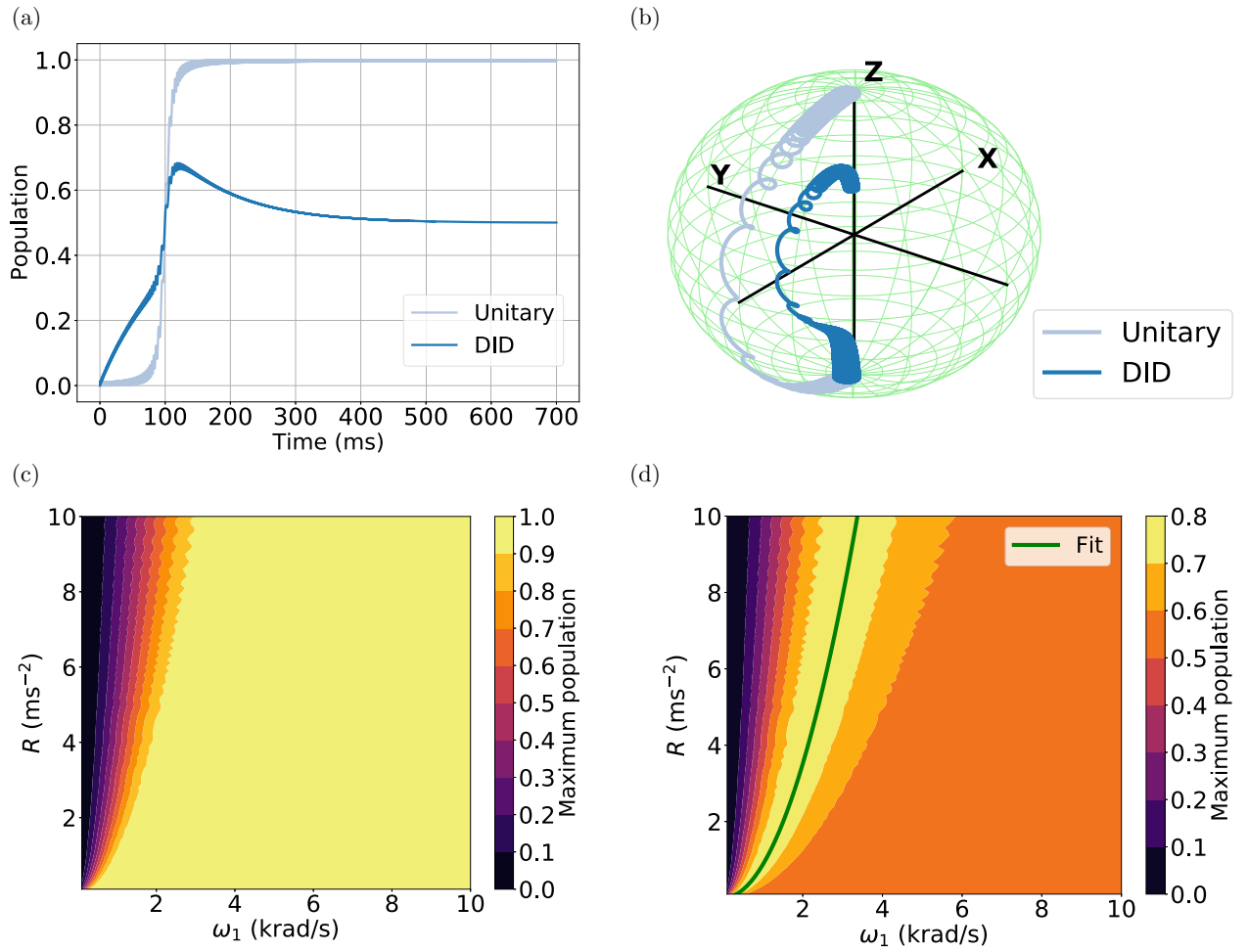

FIG. 2. Rectangular pulse. (a) The population transferred from the ground state to the excited state is plotted with respect to time for the unitary case, denoted by the light blue curve (upper curve) and the DID case, denoted by the dark blue curve (lower curve). Parameter values used are as follows: $\delta\omega = 10$ k rad/s, $\omega_1 = 1.0$ k rad/s, $R = 0.1$ ms^{-2}, $\tau_c = 10^{-2}$ ms. (b) The magnetization vector is plotted over the unit sphere for the unitary case, denoted by the light blue curve (outer curve) and the DID case, denoted by the dark blue curve (inner curve). Parameter values used are the following: $\delta\omega = 50$ k rad/s, $\omega_1 = 3.5$ k rad/s, $R = 1.0$ ms^{-2}, $\tau_c = 10^{-3}$ ms. The filled contours represent the maximum population transferred to the excited state from the ground state as a function of ω_1 and R for the (c) unitary and (d) DID cases. Here, the yellow strip indicates the optimal region where one can achieve the highest transfer in the presence of DID in the range of 0.7 to 0.8. The green line denotes the parabolic fit, which matches the numerical data well. Parameter values used: $\delta\omega = 50$ k rad/s, $\tau_c = 10^{-2}$ ms.

two fields: one is the frequency sweep $\Delta\omega(t)$ along the z direction that runs from $-\delta\omega$ to $\delta\omega$ and the other is ω_1 along the x direction. So there will be an effective field $\omega_{\text{eff}} = \sqrt{\Delta\omega^2(t) + \omega_1^2}$, about which the magnetization nutates. The magnetization vector **M** follows the effective field ω_{eff} at every instant while nutating about it.

We plot the magnetization vector over the Bloch sphere in Fig. 2(b). When $\Delta\omega(t) > \omega_1$, it remains near the z axis. As we started with the state $|g\rangle$, which is an eigenstate of σ_z with the corresponding eigenvalue -1, the magnetization vector has, initially, its z component M_z as the only nonzero Cartesian component, For the unitary case M_z runs from -1 to 1, as denoted by the light blue curve. The final value of M_z becomes 1 because we remain close to the adiabatic limit. If the adiabaticity condition were not satisfied, the final M_z would be less than 1. As the sweep progresses towards the resonance, the offset $\Delta\omega(t)$ becomes comparable to ω_1; the effective field gains a transverse component. As a consequence, M_x and M_y develop nonzero values gradually, which causes the wobbling motion over the sphere. We can see that at the resonance point, i.e., when $\Delta\omega(t) = 0$, the effective field ω_{eff} is directed exactly along the x axis. Consequently, **M** also points along the x direction at this point; as a result, only M_x survives and becomes -1. It is evident that for the unitary case, **M** moves over the surface of the sphere and tries to follow the effective field at every instant.

Here in Fig. 2(b), we plot the magnetization vector by incorporating the DID terms as well, denoted by the dark blue curve. We notice that as there is no coherence present initially, only M_z undergoes a decay in the beginning due to DID. Eventually, coherences develop and **M** starts following a trajectory *inside* the Bloch sphere. Near the resonance point, the M_x value builds up, but here again due to the effect of DID,

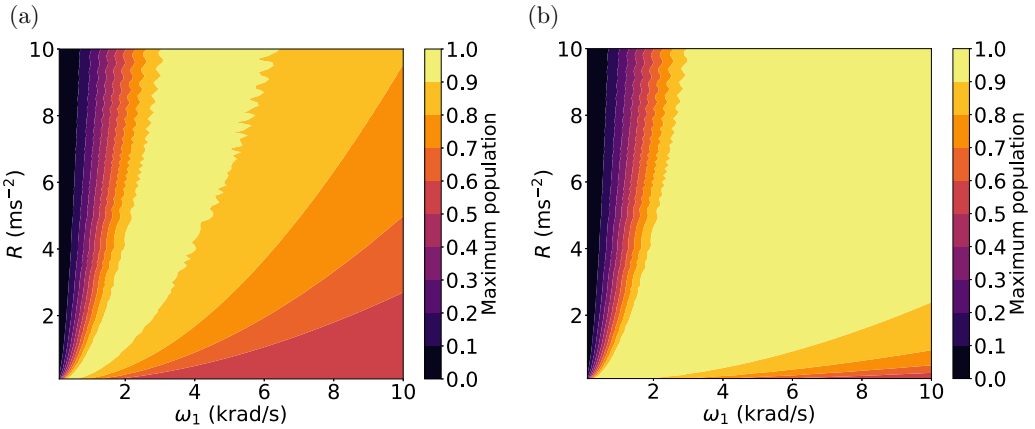

FIG. 3. Rectangular pulse. The filled contours represent the maximum population transferred to the excited state from the ground state as a function of ω_1 and R for the DID case for lower values of τ_c: (a) for $\tau_c = 10^{-3}$ ms, (b) for $\tau_c = 10^{-4}$ ms. Here, the highest possible transfer in the optimal yellow region lies in the range of 0.9 to 1.

it cannot reach its unitary value -1; so it passes through the x axis at a reduced radius. Finally, M_z approaches a steady-state value that is less than 1, as it again suffers a loss.

To observe the dependence of the population transfer on the parameters ω_1 and R, we show a contour plot of the maximum population transferred to the excited state from the ground state. From the plot in Fig. 2(c), we can infer that, for a particular R value, if we increase ω_1, the maximum population increases and after a threshold value of ω_1, it reaches the highest value 1, which means complete population transfer has taken place. On the other hand, if we fix the ω_1 value and increase the R value, we see that the maximum population suffers. This behavior of population transfer is in exact agreement with Zener's formula for transition probability given in Eq. (5). From the formula, it can be verified that when $\frac{\omega_1^2}{R} \gg 1$, we obtain better population transfer and $\frac{\omega_1^2}{R} \ll 1$ results in less population transfer.

Then we study the population behavior when DID is taken into account. In Fig. 2(d), we notice an optimal region in the plot as shown by the yellow strip, where we achieve the highest transfer, in the range 0.7 to 0.8. If we go beyond this region, the population transfer falls off. Therefore, to achieve the maximum transfer, we need to choose the parameter values R and ω_1 in such a way that we remain close to this optimal region. The behavior up to the yellow region can be explained by the LZ theory. However, it fails to explain what happens beyond this yellow region. That means the large orange region (that limits the lower range to 0.5), where DID sets in and why they reappear. This contour plot captures the competition and the crossover between the LZ effect and DID. The line of optimality separates the pre and postoptimal regions. In the preoptimal region, the LZ effect dominates and in the postoptimal region, DID dominates. We shall try to understand this kind of optimal behavior by developing a proper mathematical model in the following part of the paper.

We construct a set of ω_1 and R for the optimal population transfer. Next, we fit this set of ω_1 and R with a simple polynomial function to understand their functional dependence. The minimum power of ω_1 that fits the data is 2. Hence, we obtain $R \propto \omega_1^2$ for each point in the optimal yellow region of the contour plot in Fig. 2(d). The green line denotes this parabolic fit. It gives a good fit with the numerical data. We can explain the fit from the probability formula. When $\frac{\omega_1^2}{R} \ll 1$, the probability for population transfer (ARP) for the unitary case is given by

$$P' = 1 - \exp\left(-\frac{\pi\omega_1^2}{2R}\right) \approx \frac{\pi\omega_1^2}{2R}. \tag{13}$$

So the leading-order term in the expression of P' would be proportional to $\frac{\omega_1^2}{R}$. Thus, our fit function is taken to be $R = k\omega_1^2$ and we find that the value of the fitting parameter k is given by $k = 0.88 \pm 0.01$.

We note that the DID is responsible for the decayed transfer of population. So the maximum transfer achieved in Fig. 2(d) is less than 1. The maximum transfer value can be improved if the decay timescale of the fluctuations τ_c reduces. In Fig. 3, we study the behavior of the contour plot of maximum population transfer with respect to ω_1 and R for lower τ_c values. We find that for $\tau_c = 10^{-3}$ ms in Fig. 3(a), and for $\tau_c = 10^{-4}$ ms in Fig. 3(b), the maximum population transfer obtained is very close to the unitary value and stays within the range of 0.9 to 1. In Fig. 3(b), we can see that the optimal yellow region becomes so wide that it almost approaches the unitary behavior as obtained in Fig. 2(c).

Existence of optimality: A phenomenological study

From the contour plot in Fig. 2(d), we can see that if we move along a constant R value, the maximum population shows a nonmonotonic behavior for ω_1. At first, it increases with ω_1 (which can be explained by the LZ formula). However, after crossing the optimal yellow strip, the effect of DID becomes more prominent and we notice that the population transfer reduces with a subsequent increase in the ω_1 value. So the yellow strip shows the optimal value of ω_1, for which we get the best population transfer.

To observe this optimal behavior more concisely, we take a selected slice from the contour plot in Fig. 2(d) for a fixed R value, $R = 0.1$ ms^{-2} and plotted it with respect to ω_1 in Fig. 4. In Fig. 4, we can see that the maximum population shows optimality with respect to ω_1. When ω_1 exceeds a

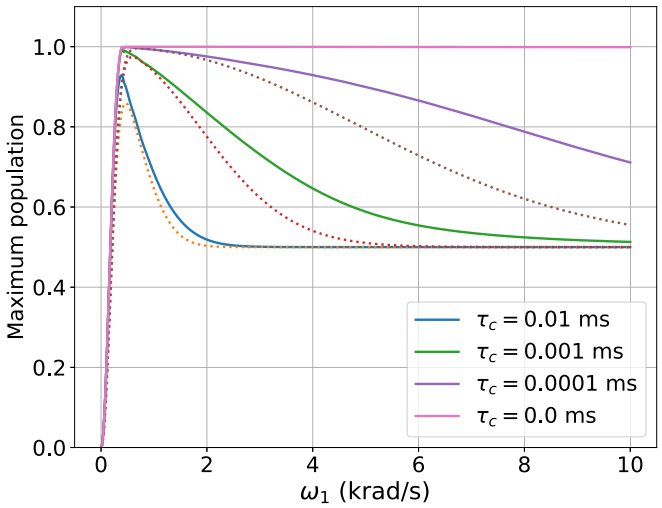

FIG. 4. Rectangular pulse. The maximum population transferred to the excited state in the presence of DID is plotted as a function of ω_1 for different τ_c values (τ_c values taken in decreasing order, from bottom to top). The dotted lines denote the maximum population curve plotted using our proposed model $p(\omega_1)$. Parameter values used: $\delta\omega = 10$ k rad/s, $R = 0.1$ ms^{-2}.

threshold value, the DID effect dominates and dictates the dynamics. Consequently, the population decreases with a further increase in ω_1 and finally saturates at the steady-state value 0.5. To check the dependence on τ_c, we did the same for various values of τ_c. As we increase τ_c, the decay becomes more and the optimal value of ω_1 gets shifted towards the origin.

As Eq. (12) does not have any closed-form analytical solution, we propose a phenomenological model which can explain the behavior shown in Fig. 2(d) qualitatively as follows:

$$\mathcal{P}(t) = \frac{1}{2}\left[1 - \exp\left(-\frac{\pi\omega_1^2}{2R}\right)\right] \times \left[1 + \exp\left(-\omega_1^2\tau_c t\right)\tanh\left(\frac{R}{\omega_1}(t - \delta\omega/R)\right)\right]. \tag{14}$$

We construct the model in the following way.

(1) We begin with the unitary case for which $\tau_c = 0$, and LZ theory provides the solution for that, i.e., $[1 - \exp(-\frac{\pi\omega_1^2}{2R})]$.

(2) The temporal behavior, as we observed in Fig. 2(a), is qualitatively captured by a phenomenological factor $\tanh(\frac{R}{\omega_1}(t - \delta\omega/R))$. Combining (i) and (ii), we get the model for the unitary case as $\frac{1}{2}[1 - \exp(-\frac{\pi\omega_1^2}{2R})][1 + \tanh(\frac{R}{\omega_1}(t - \delta\omega/R))]$.

(3) To account for the decay due to DID, we phenomenologically introduce a τ_c-dependent factor $\exp(-\omega_1^2\tau_c t)$ by multiplying it with the $\tanh(\frac{R}{\omega_1}(t - \delta\omega/R))$ term and finally arrive at the form given in Eq. (14).

This model $\mathcal{P}(t)$ predicts a maximum transfer occurring when

$$\frac{d}{dt}[\mathcal{P}(t)] = 0$$
$$\Rightarrow t_{\max} = \frac{1}{R}\left[\delta\omega + \frac{\omega_1}{2}\sinh^{-1}\left(\frac{2R}{\omega_1^3\tau_c}\right)\right]. \tag{15}$$

In Fig. 5(a), we plot the excited-state population as a function of time for the DID case. The solid blue line represents the numerically generated data and the dashed red line denotes the population curve plotted using our proposed model $\mathcal{P}(t)$. Our model provides a reasonably good match with the data, and the peaks occur nearly around the same time. Therefore, $t_{\max}$ in Eq. (15) provides a fair estimation of the occurrence of the optimal point.

Now, as we saw in Fig. 4, the chosen slices from the contour data show an optimal transfer for a certain ω_1, we use the above model with $t = t_{\max}$ to fit the slice data.

We define the maximum population at $t = t_{\max}$ as

$$p(\omega_1) = \mathcal{P}(t_{\max}) = \frac{1}{2}\left[1 - \exp\left(-\frac{\pi\omega_1^2}{2R}\right)\right] \times \left[1 + \exp\left(-\omega_1^2\tau_c t_{\max}\right)\tanh\left(\frac{R}{\omega_1}(t_{\max} - \delta\omega/R)\right)\right]. \tag{16}$$

The above Eq. (16) represents our model for the maximum population as a function of ω_1. This $p(\omega_1)$ is plotted as a function of ω_1 in Fig. 5(b), as shown by the solid green line. In this figure, the dashed blue line represents the transfer described by the conventional LZ formula for population inversion (ARP) and the dashed-dotted orange line leaves the signature of DID. When we take the product of these two, there will be a competition between these two effects: the first LZ factor will try to make the population transfer happen, whereas the second part coming from DID causes the population to decay. As a result, we get a nonmonotonic behavior as is shown by the solid green curve leading to an optimal population transfer for a certain value of ω_1.

In Fig. 4, we also plotted the optimum population as a function of ω_1 using our phenomenological model $p(\omega_1)$ for each τ_c value, as indicated by the dotted lines. Although it does not give an exact match with the numerical data, our focus is to reach close to the maximum (peak) value or the optimal region in terms of the contour plots. Therefore, the model delivers a qualitative justification for the overall behavior and successfully explains the existence of the optimal behavior in a simple way.

B. Gaussian pulse profile

Now, we shall consider a Gaussian pulse profile for the applied drive. Gaussian pulses are very effective in spin inversion and selective excitation [39–42]. Selective excitation involves applying radio-frequency pulses that affects only a certain bandwidth in the frequency spectrum. It was demonstrated that Gaussian pulses satisfy the condition of selectivity with considerable accuracy since its excitation falls off very

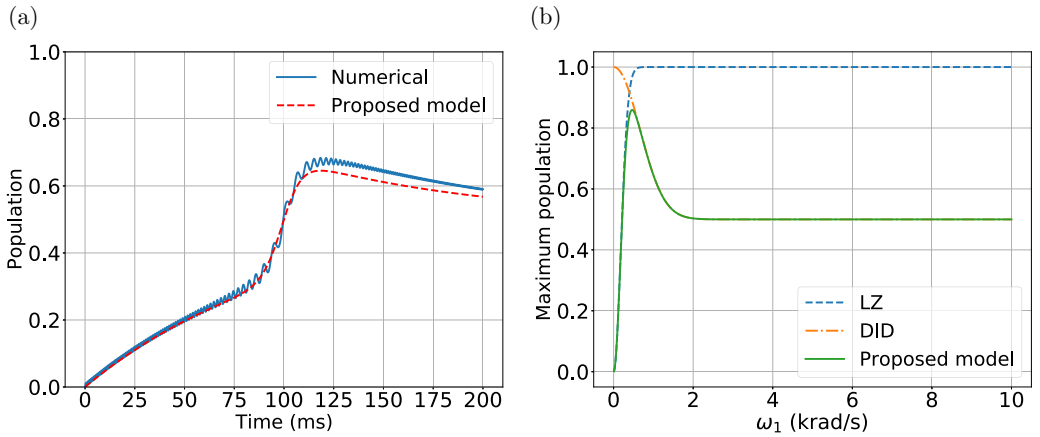

FIG. 5. Rectangular pulse. (a) The population transferred from the ground state to the excited state is plotted as a function of time. The solid blue line represents the numerical data and the dashed red line represents the population curve plotted using our proposed model $\mathcal{P}(t)$ as a function of time. (b) The maximum population transferred to the excited state for the DID case is plotted using our proposed model $p(\omega_1)$ as represented by the solid green line. The dashed blue line (the rising curve) represents the transfer described by the conventional LZ formula, and the dashed-dotted orange line (the falling curve) represents the decay in the transfer due to DID. There will be a competition between these two effects, leading to an optimal population transfer for a certain value of ω_1. Parameter values used: $\delta\omega = 10$ k rad/s, $R = 0.1$ ms^{-2}, $\tau_c = 10^{-2}$ ms.

quickly; its effect on the rest of the spectrum is minimal. They are also widely used in nuclear magnetic resonance (NMR) imaging [43]. Here we intend to study how the efficiency of ARP is influenced with the use of a Gaussian pulse.

For Gaussian pulse, the amplitude ω_1 is no longer time independent; it changes with time in the following manner:

$$\omega_1^{\text{gauss}}(t) = \omega_1^g \exp\left(-\frac{(t - T/2)^2}{\beta}\right), \tag{17}$$

where β is a measure of the width of the Gaussian and is related to the *full-width at half maximum (FWHM)* of the Gaussian σ as $\beta = \frac{\sigma^2}{4\ln 2}$.

At $t = T/2$, $\omega_1^{\text{gauss}}(t) = \omega_1^g$, which is the maximum value that the pulse profile can take. At $t = 0$ and $t = T$, $\omega_1^{\text{gauss}}(t) = \omega_1^g \exp(-\frac{(T/2)^2}{\beta})$. Let us suppose we want to cut off the Gaussian at a fraction f of the maximum. That means, at $t = 0$ and $t = T$, $\omega_1^{\text{gauss}}(t) = \omega_1^g f$. By satisfying the above-mentioned criterion, we find that $\beta = \frac{(T/2)^2}{\ln(\frac{1}{f})}$. For our simulations, we set $f = 0.1$ to truncate the Gaussian profile at 0.1 of the maximum.

To compare the system dynamics under a rectangular and a Gaussian pulse profile, we ensure that an equal amount of energy is supplied to the system for both these pulse profiles. We equate the pulse areas of these two profiles and obtain

$$\omega_1^g = \frac{\omega_1 T}{\sqrt{\pi\beta}\,\text{erf}\left(\frac{T}{2\sqrt{\beta}}\right)}. \tag{18}$$

Equation (18) provides the relation between ω_1^g and ω_1 such that the equal area condition is satisfied. This relation will be used for the subsequent simulations with a Gaussian pulse. In Eq. (17), we chose the Gaussian profile in such a way that its duration remains T, which is the same as that of the rectangular pulse profile. So, on physical grounds, we can argue that to keep the area of both these profiles constant within the same duration, the peak value (maximum) of the Gaussian ω_1^g has to be much higher than ω_1 (the maximum amplitude of the rectangular pulse). This can be verified from Eq. (18) as well by putting some numerical value for T. For $T = 200$ ms, we checked that $\omega_1^g = 1.7686\,\omega_1$, which means $\omega_1^g > \omega_1$.

In Fig. 6(a), we plot the population with respect to time. We kept the parameter values the same as that taken for the rectangular profile: $\delta\omega = 10$ k rad/s, $\omega_1 = 1$ k rad/s, $R = 0.1$ ms^{-2}. We can see that a Gaussian pulse results in a much smoother population behavior than a rectangular pulse with an equal area. Also, we note that for the same parameter values of ω_1 and R, we achieve better steady-state population transfer for the DID case, using a Gaussian pulse.

In the magnetization plot over the Bloch sphere for the DID case, shown in Fig. 6(b), we see that the magnetization vector follows a trajectory inside the Bloch sphere. In contrast to the same plot done for a rectangular pulse profile, here we note that initially M_z decays very slowly. This happens because near $t = 0$, $\omega_1^{\text{gauss}}(t) = \omega_1^g f = 0.1\,\omega_1^g = 0.17686\,\omega_1$, for our chosen parameter values; i.e., $\omega_1^{\text{gauss}}(t) < \omega_1$. As a result, it does not exhibit any significant decay along the z direction, and the overall nature of the magnetization curve is very smooth.

In Fig. 6(d), we show the contour plot of the maximum population transferred to the excited state from the ground state when DID is taken into account. Here also we obtain a similar optimal behavior of population transfer. However, the strips become narrower in this case and the highest transfer increases to 0.9. That means we achieve a more efficient transfer. In addition to that, we notice that the optimal yellow region occurs for a lower range of ω_1 values, implying that we can achieve more transfer by applying a drive of relatively lower amplitude. Therefore, frequency sweep using a Gaussian pulse results in better and more efficient population transfer. Here, we fit the contour data in the optimal yellow region with a parabolic fit, as shown by the green line. So our

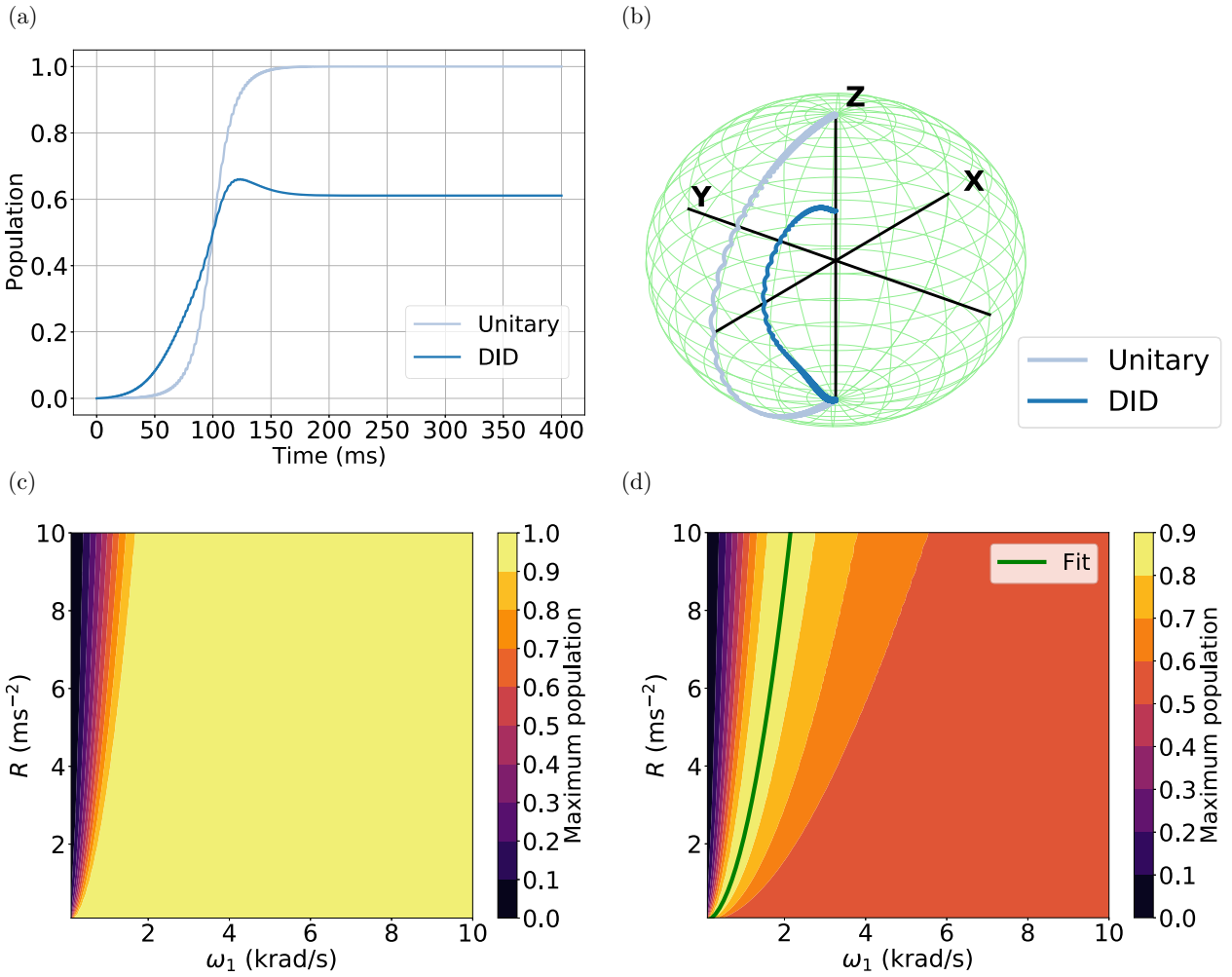

FIG. 6. Gaussian pulse. (a) The population transferred from the ground state to the excited state is plotted with respect to time for the unitary case, denoted by the light blue curve (upper curve) and the DID case, denoted by the dark blue curve (lower curve). Parameter values used: $\delta\omega = 10$ k rad/s, $\omega_1 = 1.0$ k rad/s, $R = 0.1$ ms^{-2}, $\tau_c = 10^{-2}$ ms. (b) The magnetization vector is plotted over the unit sphere for the unitary case, denoted by the light blue curve (outer curve) and the DID case, denoted by the dark blue curve (inner curve). Parameter values used: $\delta\omega = 50$ k rad/s, $\omega_1 = 3.5$ k rad/s, $R = 1.0$ ms^{-2}, $\tau_c = 10^{-3}$ ms. The filled contours represent the maximum population transferred to the excited state from the ground state as a function of ω_1 and R for the (c) unitary and (d) DID cases. Here, the yellow strip indicates the optimal region where one can achieve the highest transfer in the presence of DID in the range of 0.8 to 0.9. The green line denotes the parabolic fit, which matches the numerical data well. Parameter values used: $\delta\omega = 50$ k rad/s, $\tau_c = 10^{-2}$ ms.

fit function is taken to be $R = k\omega_1^2$ and the fitting parameter k turns out to be $k = 2.17 \pm 0.04$ for this case.

IV. DISCUSSIONS

We showed that DID affects the ARP; thus, the population transfer suffers. DID prevents the complete transfer achieved under unitary dynamics. When DID is included in the dynamics, we find an optimal value of the population transfer, which is less than 1 (for the excited state). Furthermore, this implies that since the population transfer gets reduced due to DID, the system is likely to make a transition from $E_+(t)$ to $E_-(t)$ or vice versa, which is nothing but an LZ transition.

This work shows that optimality exists in the transferring population in a TLS using a frequency sweep model. In the presence of DID, population transfer shows a nonmonotonic behavior with respect to time as well as ω_1. In the time-series plot, we observe that the population hits the maximum at a certain time, which we denote as $t_{\max}$, and gradually, it decays down to the steady-state value (which is 0.5 for rectangular pulse profile). Therefore, we need to turn off the drive at $t = t_{\max}$ to achieve the best transfer. In the contour plot of the maximum population in the R versus ω_1 plane, the yellow strip signifies the optimal region. We need to choose the parameters R and ω_1 suitably so that we can arrive at this region to obtain the most efficient transfer.

Here we choose the relaxation times T_1 and T_2 to be large, such that the decoherence due to system-environment coupling becomes negligibly small. So the nonunitary behavior originates principally due to DID. However, in situations where the system-environment coupling dominates over DID, we must include the contribution from the relaxation processes. In such cases, we would see that population transfer

is affected due to system-environment coupling. With time, the population would finally saturate at the equilibrium values $\rho_{s,11} = \frac{1+M_0}{2}$ and $\rho_{s,22} = \frac{1-M_0}{2}$.

We propose a qualitative model to explain the optimal behavior that we observe in ARP for a rectangular pulse. The factor coming from the conventional LZ formula is responsible for the initial growth in population transfer. However, as ω_1 becomes large enough to have an impact of DID on the dynamics, the transfer starts to decay with ω_1. Therefore, there exists an optimum value of ω_1 for which the transfer hits the maximum.

We extended our analysis to shaped pulses. We found that using a Gaussian pulse over a rectangular pulse is a better and more efficient option to achieve population transfer by supplying an equal amount of energy. When we look at the steady-state behavior of the population transfer as shown in Figs. 2(a) and 6(a), we can conclude that, for a Gaussian pulse, the transfer finally saturates at a higher value. This behavior can be explained in the following way: At $t = T/2$, $\omega_1^{\text{gauss}}(t)$ attains the maximum value ω_1^g and when $t > T/2$ (or $t < T/2$), the value of $\omega_1^{\text{gauss}}(t)$ eventually decreases with time. When $t = T$, $\omega_1^{\text{gauss}}(t) = \omega_1^g f = 0.1\ \omega_1^g$, for $f = 0.1$, which is definitely less than ω_1 (the amplitude of the rectangular pulse throughout the duration T). Therefore, towards the end of the Gaussian pulse, the DID is small and is insufficient to cause a saturation at 0.5. So the final steady-state value of the excited-state population remains above 0.5. It is noteworthy that, had we chosen a higher cutoff fraction for the Gaussian profile instead of $f = 0.1$, the effect of DID would have been more prominent and the steady-state behavior would look very similar to the rectangular pulse.

From the contour plots of maximum population transfer for a Gaussian pulse, we can see that in Fig. 6(d), the upper limit of the color bar has increased to 0.9, whereas for a rectangular pulse it was 0.8. Moreover, the filled contours (strips) have become narrower, smoother, and shifted towards the origin. This implies that applying a drive with a lower strength (low ω_1) can achieve better transfer using a Gaussian pulse. Therefore, a Gaussian pulse provides higher efficiency in population transfer using ARP than a rectangular pulse.

Before drawing the final conclusions, we would like to emphasize that both strong driving and environmental fluctuations are essential to witness the effect of the DID. In the entire work, we consider strong driving that satisfies the adiabaticity condition, i.e., $\omega_1^2 \gg R$. So a strong drive favors the population transfer in ARP. However, the application of a strong drive also results in a significant amount of decay due to DID, which is scaled by the timescale of decay of the environmental fluctuations (τ_c). We note that the impact of the DID is less if the correlation of the fluctuations decays very fast, i.e., $\tau_c \to 0$, which corresponds to an extreme motional narrowing regime. When $\tau_c = 0$, the DID disappears along with the dissipator arising from system-environment coupling, leading to the unitary dynamics such that complete population transfer can be achieved. The other extreme limit is $\tau_c \to \infty$. In this limit, the assumption involving timescale separation between the system and the environment will no longer hold. As such, we must abandon the Markovian picture and adopt a suitable non-Markovian description.

V. CONCLUSION

We implemented population transfer in a TLS by ARP using a linear chirped pulse while including the dissipative effects coming from the applied drive in our study. Most interestingly, we found that, even within the adiabatic limit, the population inversion suffers from the detrimental effects of DID. Further, we showed that the population transfer exhibits an optimal behavior as a result of the competing processes like the conventional LZ effect and DID. The values of ω_1 and τ_c decide the maximum value the transferred population can acquire. Not only does the temporal behavior, but the population transfer behaves nonmonotonically as a function of the sweep rate R and the drive amplitude ω_1 also. We showed that a truncated chirped pulse that stops at the point where optimality is achieved yields the best possible transfer. We proposed a phenomenological model to qualitatively explain the transfer behavior to estimate the optimal point. We analyzed both rectangular and Gaussian pulse profiles and showed that the Gaussian profile gave a more efficient result than the rectangular profile. We contemplate that our results would be beneficial for the practitioners of ARP, and they would be able to achieve the optimal population transfer in realistic experimental setups.

[1] C. Zener, Proc. R. Soc. A **137**, 696 (1932).
[2] L. D. Landau, Phys. Z. Sowjetunion **1**, 88 (1932).
[3] L. D. Landau, Phys. Z. Sowjetunion **2**, 46 (1932).
[4] M. Matsuzawa, J. Phys. Soc. Jpn. **25**, 1153 (1968).
[5] A. P. M. Baede, A. M. C. Moutinho, A. E. de Vries, and J. Los, Chem. Phys. Lett. **3**, 530 (1969).
[6] R. E. Olson, Phys. Rev. A **2**, 121 (1970).
[7] H. J. Zwally and P. G. Cable, Phys. Rev. A **4**, 2301 (1971).
[8] A. Abragam, *The Principles of Nuclear Magnetism* Vol. 32, (Oxford University Press, New York, 1961).
[9] F. Bloch, Phys. Rev. **70**, 460 (1946).
[10] L. E. Drain, Proc. Phys. Soc. A **62**, 301 (1949).
[11] G. Chiarotti, G. Cristiani, L. Giulotto, and G. Lanzi, Nuovo Cim **12**, 519 (1954).
[12] A. G. Redfield, Phys. Rev. **101**, 67 (1956).
[13] A. Abragam and W. G. Proctor, Phys. Rev. **109**, 1441 (1958).
[14] C. P. Slichter and W. C. Holton, Phys. Rev. **122**, 1701 (1961).
[15] W. R. Janzen, T. J. R. Cyr, and B. A. Dunell, J. Chem. Phys. **48**, 1246 (1968).
[16] S. Herbers, Y. M. Caris, S. E. J. Kuijpers, J.-U. Grabow, and S. Y. T. van de Meerakker, Mol. Phys. **0**, e2129105 (2022).
[17] P. R. Kaprálová-Ždánská, M. Šindelka, and N. Moiseyev, J. Phys. A: Math. Theor. **55**, 284001 (2022).

[18] J. Chen, L. Deng, Y. Niu, and S. Gong, Phys. Rev. A **103**, 053705 (2021).
[19] J. Feilhauer, A. Schumer, J. Doppler, A. A. Mailybaev, J. Böhm, U. Kuhl, N. Moiseyev, and S. Rotter, Phys. Rev. A **102**, 040201(R) (2020).
[20] A. Mukherjee, A. Widhalm, D. Siebert, S. Krehs, N. Sharma, A. Thiede, D. Reuter, J. Förstner, and A. Zrenner, Appl. Phys. Lett. **116**, 251103 (2020).
[21] J. S. Melinger, S. R. Gandhi, A. Hariharan, J. X. Tull, and W. S. Warren, Phys. Rev. Lett. **68**, 2000 (1992).
[22] J. S. Melinger, S. R. Gandhi, A. Hariharan, D. Goswami, and W. S. Warren, J. Chem. Phys. **101**, 6439 (1994).
[23] V. Malinovsky and J. Krause, Eur. Phys. J. D **14**, 147 (2001).
[24] H. Maeda, J. H. Gurian, D. V. L. Norum, and T. F. Gallagher, Phys. Rev. Lett. **96**, 073002 (2006).
[25] P. Ao and J. Rammer, Phys. Rev. Lett. **62**, 3004 (1989).
[26] P. Ao and J. Rammer, Phys. Rev. B **43**, 5397 (1991).
[27] S. Ashhab, Phys. Rev. A **94**, 042109 (2016).
[28] P. Nalbach and M. Thorwart, Phys. Rev. Lett. **103**, 220401 (2009).
[29] M. Wubs, K. Saito, S. Kohler, P. Hänggi, and Y. Kayanuma, Phys. Rev. Lett. **97**, 200404 (2006).
[30] Z. Sun, L. Zhou, G. Xiao, D. Poletti, and J. Gong, Phys. Rev. A **93**, 012121 (2016).
[31] R. S. Whitney, M. Clusel, and T. Ziman, Phys. Rev. Lett. **107**, 210402 (2011).
[32] A. Chakrabarti and R. Bhattacharyya, Phys. Rev. A **97**, 063837 (2018).
[33] J. R. Rubbmark, M. M. Kash, M. G. Littman, and D. Kleppner, Phys. Rev. A **23**, 3107 (1981).
[34] A. Chakrabarti and R. Bhattacharyya, Europhys. Lett. **121**, 57002 (2018).
[35] N. Chanda and R. Bhattacharyya, Phys. Rev. A **101**, 042326 (2020).
[36] N. Chanda and R. Bhattacharyya, Phys. Rev. A **104**, 022436 (2021).
[37] A. Chatterjee and R. Bhattacharyya, Phys. Rev. A **102**, 043111 (2020).
[38] S. Saha and R. Bhattacharyya, J. Phys. B: At. Mol. Opt. Phys. **55**, 235501 (2022).
[39] C. Bauer, R. Freeman, T. Frenkiel, J. Keeler, and A. J. Shaka, J. Magn. Reson. **58**, 442 (1984).
[40] H. Kessler, H. Oschkinat, C. Griesinger, and W. Bermel, J. Magn. Reson. **70**, 106 (1986).
[41] L. Emsley and G. Bodenhausen, Chem. Phys. Lett. **165**, 469 (1990).
[42] R. Bhattacharyya and L. Frydman, J. Chem. Phys. **127**, 194503 (2007).
[43] R. J. Sutherland and J. M. S. Hutchison, J. Phys. E **11**, 79 (1978).